Validation of a SAR-Only Wind-Vector Retrieval Against Shipborne In Situ Wind Observations in the European Arctic

Mathias Tollinger and Rune Grand Graversen

***Abstract*—Space-borne synthetic aperture radar (SAR) observations provide broad coverage of high-resolution snapshots of the sea surface conditions in polar regions. However, their potential has not yet been fully harnessed for meteorological applications. For instance, standard methods for SAR wind-vector retrieval rely on wind direction inputs from numerical weather prediction models, which hampers the high-resolution capabilities of SAR wind retrievals and the use of these in data assimilation. A recently proposed SAR-only wind-vector retrieval method, that uses SAR information more exhaustively than standard methods do, is compared to *in situ* ship observations and is found to perform similarly to a standard method under average wind conditions at open sea. However, in coastal regions, at high wind speeds, and in complex meteorological conditions this new application outperforms the standard method. It is concluded here that wind fields obtained from the SAR-only wind-vector retrieval are suitable for data assimilation in high-resolution weather prediction models, since they can provide model-independent, high-quality, and high-resolution observational wind information. In addition, a simple interpolation technique is introduced to substitute land in the calibration procedure of the Doppler centroid anomaly for open-ocean SAR scenes.**

***Index Terms*—Sentinel 1, synthetic aperture radar (SAR), validation, wind retrieval.**

I. Introduction

SPACEBORNE Synthetic Aperture Radar (SAR) images show sea surface conditions in great detail. The sub-kilometre scale structures of the ocean surface detectable in SAR backscatter images are mainly a result of resonant Bragg-scattering by wind-induced surface ripples on the scale of the radar wavelength (5-6 cm for a centre frequency of 5.405 GHz [1]). The relationship between wind speed and direction, and the intensity of radar backscatter is exploited to retrieve the surface wind field from SAR measurements of the water surface.

Conventionally, wind-vector retrieval is based on the co-polarised radar backscatter signal, a radar signal transmitted and received in the same polarisation plane, vertical-vertical (VV), or horizontal-horizontal (HH) (See [2] for a detailed description of the conventional wind-vector retrieval method). Extensive work has been devoted to developing Geophysical Model Functions (GMFs) that relate the surface backscatter signal to the wind vector, e.g. [3]–[7]. GMFs that relate the comparably weak signal of the cross-polarised radar backscatter (VH or HV) to wind speed are virtually independent of wind direction and can, therefore, easily be inverted to yield wind speed only [4], [5]. The co-polarised radar backscatter signal is stronger than the cross-pol signal, but since it depends on both the speed and direction of the surface wind, wind-vector retrieval by inversion of a GMF is underdetermined. This has generally been circumvented by including wind direction information from an external source, usually a numerical weather prediction (NWP) model, as a separate cost function term during the probabilistic wind retrieval to arrive at a complete wind-vector field [2]. However, in the vicinity of complex terrain and in small-scale dynamic weather situations, the wind field from NWP models can locally be subject to large errors and hence be completely different from the real wind field captured by SAR. This is either because models fail to simulate the complexity of real meteorological phenomena, or they simulate realistic meteorological features at a wrong location or time.

In particular at high latitudes, where SAR coverage is ample, accurately predicting mesoscale ($\mathcal{O}$(1 km)–$\mathcal{O}$(100 km)) meteorological phenomena, such as polar lows is challenging for NWP models [8]. Polar lows are intense, short-lived ($\mathcal{O}$(1 day)) mesoscale cyclones that develop rapidly in maritime air during *e.g.* cold-air outbreaks over open water and are typically associated with heavy snowfall and strong winds [9]. One reason for the weak model performance is that NWP models lack quality observations at the relevant temporal and spatial scales of polar lows, which through data assimilation nudge models towards the observed reality [10]. It would be highly beneficial to obtain surface winds from SAR data without the customary use of auxiliary model-wind direction during the retrieval procedure. In that way surface wind fields obtained from SAR images are independent of NWP models and may be eligible for data assimilation, among other applications. Model-independent wind fields derived from SAR can potentially enhance NWP forecasts of polar lows by providing high-resolution observations to data assimilation.

Recently a SAR-only wind-vector retrieval method has been proposed that combines the co-pol, and cross-pol channels

Manuscript received 28 August 2023; revised 19 October 2023 and 28 November 2023; accepted 16 December 2023. Date of publication 5 January 2024; date of current version 22 January 2024. This work was supported by the Centre of Integrated Remote Sensing and Forecasting for Arctic Operations (Cirfa) through the Research Council of Norway (RCN), under Grant 237906. (Corresponding author: Mathias Tollinger.)

Mathias Tollinger is with the Complex Systems Modeling Group, Institute for Physics and Technology, The Arctic University of Norway (UiT), 9019 Tromso, Norway (e-mail: mathias.tollinger@uit.no).

Rune Grand Graversen is with the Complex Systems Modeling Group, Institute for Physics and Technology, The Arctic University of Norway (UiT), 9019 Tromso, Norway, and also with the Norwegian Meteorological Insitute, 9293 Tromsø, Norway.

with the Doppler centroid anomaly (DCA) of the radar signal providing a high-resolution wind-vector field that is independent of wind direction information from external sources [11]. Note, that this SAR-only wind-vector retrieval is different from earlier model-independent wind speed retrievals, which do not yield wind direction information and are generally based exclusively on the cross-pol channel, e.g. [4], [5], [12], [13]. Despite having a directional ambiguity, this SAR-only wind-vector retrieval produced a plausible wind field in the case study of a polar low [11]. Yet, the SAR-only wind-vector retrieval remains to be thoroughly validated against *in situ* observations and compared to the standard co-pol wind-vector retrieval method and NWP simulations, which is undertaken here.

The main source of *in situ* observations for the development of GMFs and the validation of wind retrievals from active microwave backscatter (SAR and scatterometer) has been buoy wind measurements [14]–[19]. Also an offshore mast in the North Sea has been used for this purpose [20], [21]. In addition to *in situ* observations, SAR wind retrievals have been validated against other remote sensing observations such as scatterometer retrieved winds [22], [23], airborne Stepped Frequency Microwave Radiometer (SFMR) [24], LiDAR wind measurements [25], soil moisture active and passive mission (SMAP) [6], and NWP models [3]. Despite a somewhat lower accuracy compared to offshore mast and buoy observations, shipborne *in situ* wind measurements are more prevalent and cover both the open sea and coastal regions, making them a compelling reference for validation of SAR wind retrievals and NWP models. In the case of wind resource assessment [21], both shipborne and buoy wind measurements were deemed insufficiently accurate for GMF development [26] and SAR wind retrieval validation due to sensor blockage by the ship and sensor motion. However, the abundance and broad spatial coverage make shipborne wind measurements ideal as a common reference for comparing different data sets under a variety of meteorological conditions, although care must be taken using such data as a ground truth for the development of geophysical model functions or for the intricate validation of retrieval methods for individual locations. Shipborne wind measurements and SAR wind retrievals have previously been compared in the marginal ice zone near Svalbard within the confines of a case study [27].

Here, we compare 10-m wind measurements from shipborne automated weather stations between May 2021 and October 2022 to 10-m wind from the SAR-only retrieval [11] and the standard SAR wind retrieval method that depends on auxiliary NWP wind direction. Additionally, we compare the *in situ* observations to two operational NWP models, the global model that supplies the auxiliary wind direction to the standard wind-vector retrieval, and a high-resolution regional NWP model adapted for arctic applications.

II. Materials and Methods

A. Data

1) In situ observations: *In situ* wind measurements for validation come from three types of sources: Three Norwegian Coast Guard vessels, four research vessels, and three tourist fjord-cruise ships serving daily trips on Isfjorden, Svalbard. The main difference between the observations by the Coast Guard vessels and the ones from research vessels is that data access of the Norwegian Coast Guard measurements is restricted, while data from the research vessels are openly accessible. Both were accessed via the Norwegian Meteorological Institute [28]. Coast Guard and research (C&R) vessels navigate the open ocean, which reduces the impact of topography on their respective wind readings (see Fig. 1). The wind observations from aboard tourist fjord-cruise ships on Svalbard are the Mobile Stations part of the Isfjorden Weather Information Network (IWIN) project by the University Centre in Svalbard (UNIS) [29]. IWIN mobile measurements are all taken on Isfjorden which is surrounded by complex topography including steep mountains exceeding 1000 masl (see Fig. 2) and large glaciers. The wind-sensor heights of

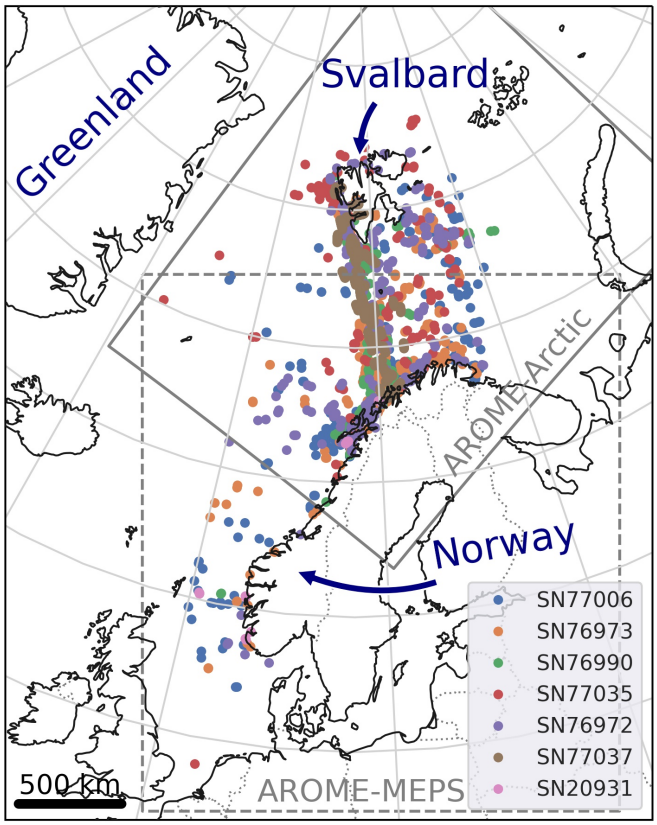

Fig. 1. Map of the European Arctic with the extent of the AROME-Arctic domain marked with a solid grey frame, and the extent of the AROME-MetCoOp domain with a dashed grey frame. Locations of the *in situ* wind measurements collected by Coast Guard and research (C&R) vessels are shown in colour for individual observation platforms with their respective station identification number in the legend.

the shipborne measurements range from 16 m to 40 m. For comparison with SAR wind retrievals and 10-m model wind, all *in situ* observations were converted to 10-m equivalent wind by applying a logarithmic wind profile in accordance with a simple approach in [30]. For conversion the logarithmic wind profile, Equation 1, together with the Charnock relation, Equation 2 [31], were iterated to find the effective roughness

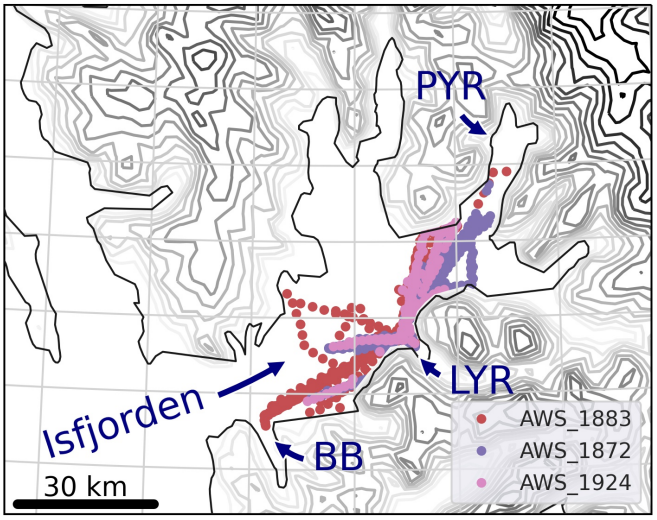

Fig. 2. Map of Isfjorden on the west coast of Svalbard, which is included in the AROME-Arctic domain. Locations of the IWIN wind measurements by the tourist fjord-cruise ships running from Longyearbyen (LYR) to the ports of Pyramiden (PYR) and Barentsburg (BB) are shown in colour with their respective identification number in the legend. Contours of the AROME-Arctic model topography are shown in 75-m intervals with the darker grey contours indicating high elevation.

length z_{0u}, starting from z_{0u}=0.0001.

$$u(z) = \frac{u_*}{\kappa} ln\left(\frac{z}{z_{0u}}\right) \quad (1) \qquad z_{0u} = \alpha \frac{u_*^2}{g} \quad (2)$$

Here, u_* is the friction velocity, κ is the Von Karman constant (0.4), z is the measurement height, α the Charnock parameter (0.0185), and g the gravitational acceleration (9.81 m s^{-2}). The minimum effective roughness length was set to 0.0002 m as in [30]. Then the equivalent neutral wind at 10 m was computed by

$$u_{10} = u(z) \frac{ln\left(\frac{10}{z_{0u}}\right)}{ln\left(\frac{z}{z_{0u}}\right)} \quad (3)$$

2) Sentinel-1 SAR images: The C-band SAR data used here were collected by the SAR instruments aboard the two identical polar orbiting satellites (Sentinel-1 A/B) of the European Space Agency's (ESA's) Sentinel-1 mission [32]. Both satellites were in the same orbital plane with a 180 ° phase difference. However, Sentinel-1 B ceased delivering observations on 23 December 2021. When both were operational, this constellation could potentially cover most of the European Arctic in all weather conditions, twice daily, on a descending (southward) morning pass, and an ascending (northward) evening pass. In practice, even before Sentinel-1 B stopped operating, this potential was never realised due to alternation between different observation modes, resulting in missing data in transition zones between land and ocean. For ocean applications in the European Arctic, the ascending evening pass is especially affected by such data losses. All SAR-related data used here are contained in ESA's Sentinel-1 Level-2 OCN product on a 1×1 km grid, as are the NWP model winds that were used as auxiliary wind information during the standard wind-vector retrieval. The Level-2 OCN products are freely available from ESA [33]. SAR-only wind vectors were retrieved from noise-corrected Normalised Radar Cross Sections (NRCSs) and Doppler Centroid (DC) frequencies. To calibrate the Doppler Centroid Anomaly (DCA), the median DC over land is subtracted from DC over water. Since not all SAR images cover a sufficient amount of land for calibration, the procedure shown in Figure 3 was applied: If a SAR scene has less than 5% valid land pixels, the DC value over land is interpolated from a time series of median DC values of all land-containing SAR scenes from coastal areas in the Arctic during 23 February 2021 to 31 October 2022. Hence the interpolation of DC over land is based on a subset of the time series that matches the particular observation constellation of the SAR scene in question. These observation constellations are a combination of observation platform (Sentine-1 A/B), beam mode (EW or IW), and polarisation (dual horisontal, HH+HV, or dual vertical, VV+VH). This procedure has to be implemented to compensate for the annual and daily variability of DC measurements and sudden offsets due to *e.g.* temperature regulation of the satellite, which are apparent in Figure 4. It was tested that different observation constellations of platform, beam mode, and polarisation, used during wind retrieval did not substantially impact the SAR-only wind-vector retrieval data.

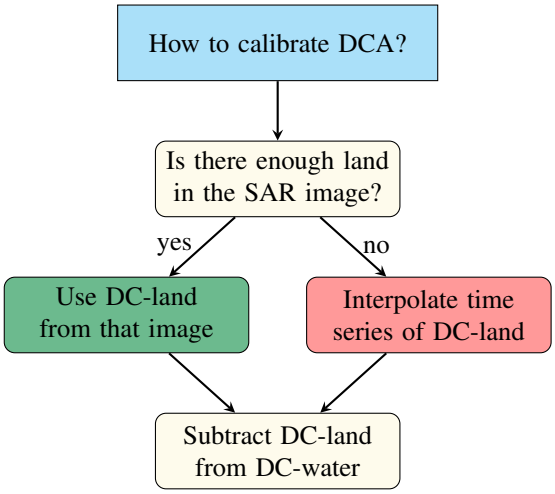

Fig. 3. Diagram of the stepwise process described in Section II-A2 to calibrate the DCA for SAR images that lack sufficient land pixels.

3) NWP models: In situ wind measurements are compared to two operational NWP models, the global high-resolution NWP model from the European Centre for Medium-Range Weather Forecasts (EC_HRES) with at least a 0.125 ° (ca 9 km) resolution [34], [35] and the high-resolution regional forecasting model AROME-Arctic with a 2.5 km resolution [20]. 10-m wind from the EC_HRES model is used as auxiliary wind information for the conventional SAR wind-vector retrieval and both, model and retrieval winds, are included

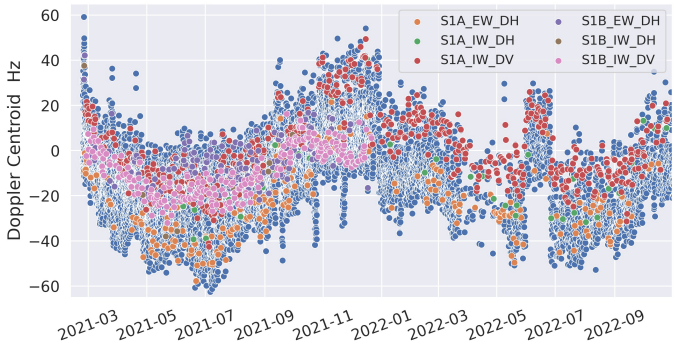

Fig. 4. Time series from 23 February 2021 to 31 October 2022 showing median DC values over coastal regions in the Arctic for more than 12000 land-containing SAR scenes in blue. Interpolated DC values are colour-coded for various SAR observation constellations that were used here to calibrate DCA for SAR scenes that lack sufficient land pixels.

in the Sentinel-1 OCN product. The AROME-Arctic model is an operational high-resolution regional forecasting system that is adapted for the European Arctic and is similar to the main Scandinavian NWP operational model AROME-MetCoOp used operationally in a collaboration between the Norwegian Meteorological Institute (MET Norway) and the Swedish Meteorological and Hydrological Institute (SMHI), [36]. To increase the size of the data set used for comparison, the AROME-Arctic domain is extended by the AROME-MetCoOp domain to cover the southern Norwegian Sea and the North Sea (see Fig. 1). For simplicity, the two models are considered the same here. Due to the high resolution of AROME-Arctic, it can realistically model mesoscale weather phenomena like polar lows and downslope windstorms. High model resolution implies a more accurate representation of the real topography which causes terrain flow such as downslope windstorms. However, at open sea where little terrain effects prevail, accurate model representation of small-scale weather disturbances is hampered by the limited availability of observations for data assimilation.

B. SAR-only wind-vector retrieval

The probabilistic SAR-only wind-vector retrieval used here is based on adaptations to the conventional Bayesian wind-vector retrieval [2] which were suggested in Tollinger et al. [11]. Auxiliary wind vector terms of the conventional Bayesian wind-vector retrieval were replaced with terms for cross-pol backscatter and DCA. Thus, the retrieved wind vector minimises the following cost function:

$$J(\theta,\mathbf{v}) = \underbrace{\left(\frac{\sigma^0_{\mathrm{MS1A}}(\theta,|\mathbf{v}|)-\sigma^0_{\mathrm{XP}}}{\Delta\sigma_{\mathrm{XP}}}\right)^2 \cdot 2w(\theta,\sigma^0_{\mathrm{XP}}) +}_{\text{cross-pol term}}$$
$$\underbrace{\left(\frac{\sigma^0_{\mathrm{CMODx}}(\theta,\mathbf{v})-\sigma^0_{\mathrm{CoP}}}{\Delta\sigma_{\mathrm{CoP}}}\right)^2 \cdot 2(1-w(\theta,\sigma^0_{\mathrm{XP}})) +}_{\text{co-pol term}}$$
$$\underbrace{\left(\frac{\mathrm{DCA}_{\mathrm{gmf}}(\theta,\mathbf{v})-\mathrm{DCA}}{\Delta\mathrm{DCA}}\right)^2}_{\text{Doppler term}} \tag{4}$$

Here the GMF for co-pol backscatter, symbolised by $\sigma^0_{\mathrm{CMODx}}(\theta,\mathbf{v})$, is either CMOD5.N [3] for VV (CMOD5.N is chosen here because this GMF is used in for the conventional SAR wind-vector retrieval [37]), or CMODH [7] for HH polarisation. The GMF for the Doppler centroid anomaly is $\mathrm{DCA}_{\mathrm{gmf}}(\theta,\mathbf{v})$ [38]. $\sigma^0_{\mathrm{CMODx}}(\theta,\mathbf{v})$ and $\mathrm{DCA}_{\mathrm{gmf}}(\theta,\mathbf{v})$ are both functions of the incidence angle, θ, and the full wind vector $\mathbf{v}$, hence, wind speed $|\mathbf{v}|$ and wind direction ϕ (see, Fig 5). Contrarily, the cross-pol GMF used here, symbolised by $\sigma^0_{\mathrm{MS1A}}(\theta,|\mathbf{v}|)$, is MS1A [6] which is a function of θ and the wind speed, $|\mathbf{v}|$, only. Subscripts XP and CoP stand for quantities related to the cross-pol and co-pol channels, respectively. Thereby, σ^0_{CoP} and σ^0_{XP}, are the measured co-pol backscatter in HH or VV polarisation and the measured cross-pol backscatter, while DCA is the measured Doppler centroid anomaly. The corresponding Gaussian error standard deviations in the denominators are $\Delta\sigma_{\mathrm{CoP}}$, $\Delta\sigma_{\mathrm{XP}}$, and ΔDCA. Previously the following constant values have been suggested for those errors, $\Delta\sigma_{\mathrm{CoP}} = 0.1$ dB [6] and $\Delta\mathrm{DCA} = 5$ Hz [39]. However, constant errors effectively give constant weight to each of the three cost function terms. This is not desirable, in particular for the cross-pol and co-pol terms that should ideally act in a complementing manner, with the co-pol term outweighing the cross-pol term at low wind speed where the co-pol signal is stronger than that of the cross-pol channel. Contrarily at high wind speed where the co-pol signal saturates and cross-pol excels, equal weight between the two terms is not desirable. Ideally well-defined variable errors would act as weighing factors for the individual costfunction terms, however here, we chose to add a simple smooth weighing function, $w(\theta,\sigma^0_{\mathrm{XP}})$ depending on the incidence angle, θ, and the crosspol backscatter σ^0_{XP}, for the transition from co-pol to cross-pol over the wind speed interval 4 - 20 m s^{-1}(details of $w(\theta,\sigma^0_{\mathrm{XP}})$ are described in the appendix). A factor 2 in $2w(\theta,\sigma^0_{\mathrm{XP}})$ and 2(1-$w(\theta,\sigma^0_{\mathrm{XP}})$) is added in Equation 4 to maintain the relative importance of the Doppler term compared to the sum of the two other costfunction terms conforming with the approach in [39].

Figure 5 shows a conceptual illustration of the method used to retrieve the SAR-only wind vectors with two solutions for the wind direction of which one is aligned with the real wind field. Even though the co-pol signal does depend on wind direction (elliptical shape in Fig. 5), in a conceptual context it

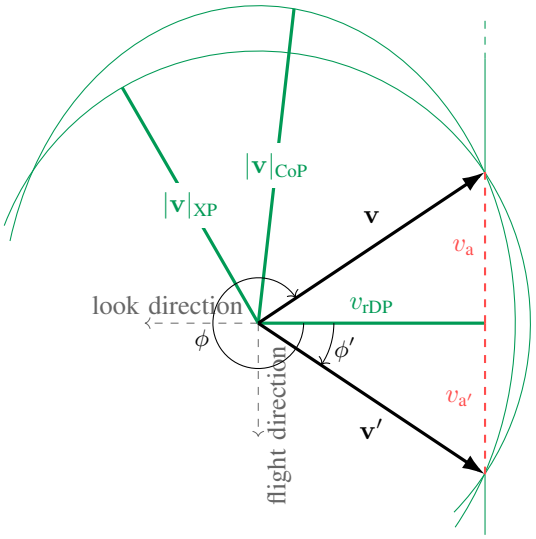

Fig. 5. Illustration of the wind vector components retrieved by the SAR-only wind-vector retrieval. Subscripts XP, CoP and DP stand for cross-pol, co-pol and Doppler, respectively, indicating the three sources of SAR information. $|\mathbf{v}|_{\mathrm{XP}}$ and $|\mathbf{v}|_{\mathrm{CoP}}$ are obtained from cross-pol and co-pol backscatter which provide mainly wind-speed information, while DCA contributes information about the wind direction via the wind vector component in range (look) direction, v_{rDP}. $\mathbf{v}$ is the full wind vector and v_{a} the wind vector component in azimuth direction (flight direction). Measured components are shown in green while unknown components are shown in red. ϕ is the wind direction relative to the range (look) direction towards the SAR instrument. Ambiguities are denoted by primed quantities.

can be assumed that both the co-pol and cross-pol terms in Equation 4 provide mainly information about the wind speed $|\mathbf{v}|_{\mathrm{CoP}}$ and $|\mathbf{v}|_{\mathrm{XP}}$, respectively. The Doppler term provides information about the wind vector component in range direction $\mathbf{v}_r$, hence parallel to the radar look direction. Since the wind component parallel to the azimuth direction (flight direction) $\mathbf{v}_a$ is not known, a wind direction ambiguity remains that is symmetrical about the range direction. Alternatively, the thin green lines in Figure 5 can be interpreted as the line representing the minima of the three cost function terms in Equation 4. Therefore, the retrieved wind vectors lie at the intersections of the minima-lines at which $J(\theta, \mathbf{v})$ has two global minima.

III. Results

All *in situ* wind measurements were taken by automated weather stations aboard ships. Nevertheless, the IWIN measurements administered by UNIS are different from the others in several ways. The tourist fjord-cruise ships in the IWIN program, carrying the UNIS weather stations, generally take the same daily routes on Isfjorden, a fjord that is bordered by complex topography including mountains above 1000 masl and several large glaciers. The remaining observations from aboard Coast Guard and research (C&R) vessels are generally taken at open sea where wind conditions predicted by the NWP models are more likely to be correct. Because the IWIN measurements are available at a higher frequency than the other observations, more collocations per SAR image can be obtained within a 1-hour observation window. Since one of the directional ambiguities of the SAR-only retrieval is assumed to be aligned with the wind field, subsequently only the ambiguity closer to the observed wind direction is shown.

A. Coast Guard & Research Vessels

Figure 1 shows the locations of all the wind measurements that are compared to SAR retrievals and NWP wind simulations. A majority of 74% of measurements were taken at open sea more than 15 km off the closest coast in the Norwegian, Barents, and North Seas. Only observations that lie in either of the AROME-Arctic and AROME-MetCoOp domains are used for comparison here.

The agreement of SAR products and NWP models with *in situ* wind speed measurements is similar in Figure 6. Wind speed estimates from the conventional SAR wind-vector retrieval generally agree the best with the ship measurements, with a mean absolute error (mae) of 1.70, a correlation coefficient (corr) of 0.86, and a root-mean-square error (rmse) of 2.25, as compared to the other three products (Fig. 6 and Tab. I). Nonetheless, there is a distinct cluster of data points that is overestimated by the conventional wind-vector retrieval with the highest retrieved wind speed of 30.2 m s^{-1}compared to measured 20.1 m s^{-1}(**X**-marker in Fig. 6b). This cluster lies within the wind speed region, $\gtrsim$20 m s^{-1}, where signal saturation of the co-pol backscatter becomes an issue for conventional wind-vector retrieval techniques that only use the co-pol channel.

The EC_HRES model, which is used to provide *a priori* wind input to the conventional SAR wind-vector retrieval, shows both the largest mean errors and most extreme outliers relative to the ship observations (Tab. I) and it underestimates some of the *in situ* wind speed observations dramatically. The largest difference between EC_HRES and observed wind speed, 18.5 m s^{-1}, is marked by triangle symbols in Figure 6c and Figure 7 and is linked to a small-scale frontal feature which is misrepresented by the coarse-resolution EC_HRES model. Some other large differences are linked to terrain flow, unresolved by EC_HRES, in coastal areas of northern Norway (not shown). Even though AROME-Arctic has almost 4 times higher resolution than EC_HRES, it suffers from similar misrepresentation errors. For instance the largest absolute difference between observed wind speed and the wind speed modelled by AROME-Arctic, 12.2 m s^{-1}, is due to a misplaced frontal zone ($+$-symbols in Figure 6d and Figure 7). Apart from such exceptional model errors, AROME-Arctic is with mea = 1.81, bias = -0.61, corr = 0.83 and rmse = 2.38 much closer to the C&R vessel observations than is EC_HRES.

The SAR-only retrieval best represents the largest *in situ* wind speed measurement, 25.7 m s^{-1}(marked by star symbols in Figures 6 and 7a) compared to the three other products as well as being close to observations for the mentioned extreme cases marked by **X**-, triangle-, and $+$-markers. The largest wind-speed differences between SAR-only retrieval and observations marked by the diamond symbol in Figure 6a is related to bright-target contamination due to inaccuracies in the valid-data mask contained in the OCN product (not shown). On average for the C&R observations the SAR-only

wind speed has the smallest bias (0.05 m s^{-1}) of all for products, but has a lower correlation coefficient (0.79), and larger errors (mae = 2.00 and rmse = 2.56) than the conventional SAR retrieval and AROME-Arctic.

With respect to wind direction the conventional SAR wind-vector retrieval (Fig. 8b) and NWP model simulations (Fig. 8c,d) agree marginally better with the C&R *in situ* wind direction measurements than does the SAR-only wind-vector retrieval (Fig. 8a and Tab. I). Wind direction from the conventional SAR wind-vector retrieval is almost identical with the NWP wind direction from EC_HRES, which is expected since it is used as auxiliary information during the conventional wind retrieval. For the wind directions from the SAR-only retrieval the directions parallel with range direction (radar look direction) are marked as red and blue shading in Figure 8a for ascending and descending orbits, respectively. In the case of poorly calibrated DCA, SAR-only retrieved wind directions have a tendency to incorrectly attain directions indicated by those shaded areas because the range wind components in these cases become too large and hence dominant (see discussion in Sec. IV and Fig. 5). The misplacement of frontal zones seen in Figure 7 caused large differences of wind speed, however, only the wind direction associated with the triangle symbols is with 52 ° exceptionally different from the *in situ* wind direction measurements (Fig. 8c). It can be noted that the difference in wind direction for the triangle symbol, associated with the largest wind speed difference between EC_HRES and observation, is lager for the conventional SAR retrieval method compared to the EC_HRES which was used as auxiliary wind information during the conventional retrieval (see Figure 8b,c). The incorrect auxiliary wind information from EC_HRES apparently corrupted the conventional SAR retrieval in this case.

Compared with the C&R vessel observations, the model-independent SAR-only wind-vector retrieval has slightly larger statistical errors than the conventional SAR wind-vector retrieval which relies on wind information from the EC_HRES model, even though the SAR-only retrieval is closer to observed wind vectors for all the cases of large errors of the other three products, shown by special markers in Figures 6–8.

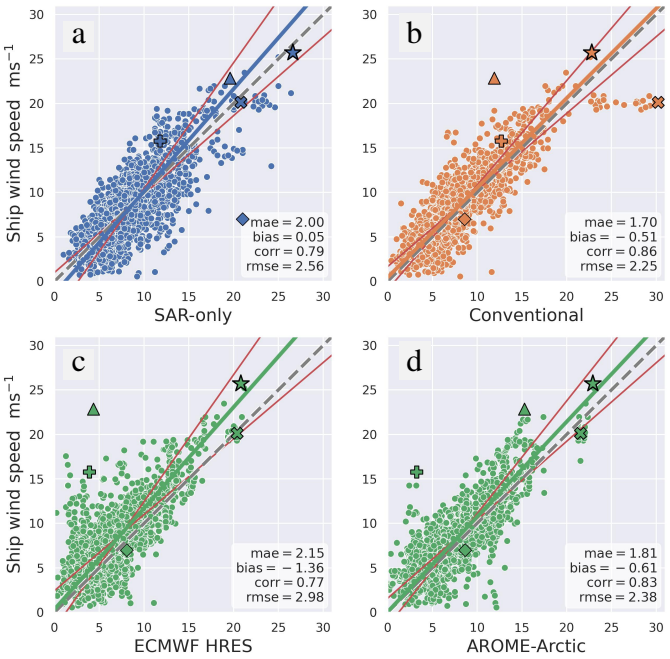

Fig. 6. Comparison of 10-m wind speed measurements from the C&R vessels with 10-m wind speed from the SAR-only wind-vector retrieval in blue (**a**), the conventional SAR wind-vector retrieval in orange (**b**) and NWP model wind speed in green from the global EC_HRES model (**c**) and the regional AROME models (**d**). Some extreme values of the data are emphasised by differently shaped black-framed markers, the largest *in situ* wind speed observation 25.7 m s^{-1} with stars, the largest conventionally retrieved winds 30.2 m s^{-1} with **X**-markers, and the largest differences between ship observations and EC_HRES or AROME with triangles (Δ= 18.5 m s^{-1}) or +-symbols (Δ= 12.5 m s^{-1}), respectively. The largest difference between observations and SAR-only retrieved wind speed (Δ= 14.0 m s^{-1}) is indicated with a diamond symbol. A linear orthogonal distance regression is shown by the thick coloured line and ordinary linear regression fits for vertical and horizontal residuals are shown by thin red lines. The grey, dashed, diagonal line indicates perfect match with measured wind. Mean absolute error (mea), bias, the Pearson correlation coefficient (corr), and the root-mean-square error (rmse) are presented in the lower right corner of every panel.

B. IWIN observations

Representing the mobile-observations part of the IWIN program on Isfjorden, Svalbard, three tourist fjord-cruise ships equipped with automatic weather stations of the type Gill MaxiMet GMX500 were measuring wind during the 2021 and 2022 summer seasons. Figure 2 shows the locations of the IWIN measurements that are compared with wind retrieved from SAR images and simulated by NWP models. Terrain elevation shown by grey contours in Figure 2 indicate the terrain as resolved by the AROME-Arctic model with the darkest contours exceeding 1000 masl. The entrance of Isfjorden and the locations of Longyearbyen (LYR), the main settlement on Svalbard, Barentsburg (BB), and the abandoned mining settlement of Pyramiden (PYR) are all marked by arrows. The fjord cruises usually follow routes departing in the morning from LYR to one of the other locations, BB or PYR, and returning to LYR in the evening.

The maximum measured wind speed of the IWIN observations in Isfjorden (Fig. 9), at 15.6 m s^{-1}, is almost 10 m s^{-1} less than the maximum measured wind speed from the C&R vessel data set, and falls short of the wind speed range, $\gtrsim$ 20 m s^{-1}, where the SAR-only retrieval can be expected to outperform the conventional wind retrieval due to its strong-wind capability that is achieved by combining co-pol and cross-pol signals. Even though the EC_HRES wind information that enters the conventional wind-vector retrieval does not represent the complexity of the wind field in Isfjorden, clearly seen in Figure 10c-f, at wind speeds $\lesssim$ 20 m s^{-1} the conventional wind-vector retrieval is not as sensitive to wind direction errors from EC_HRES as it is at high wind speed, and therefore, with respect to wind speed, it still performs marginally better than the SAR-only retrieval. Nonetheless, the two SAR retrievals behave similarly compared to the IWIN *in situ* wind speed measurements in Isfjorden as they do relative to the *in situ* observations from C&R vessels. In contrast, NWP models have difficulty simulating measured

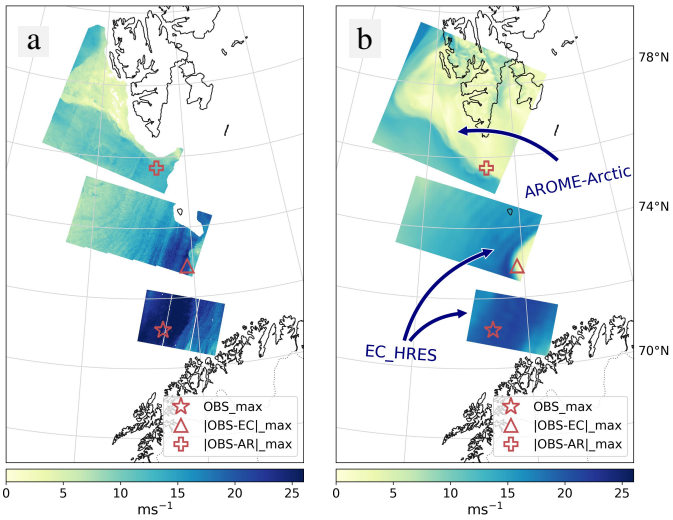

Fig. 7. Map of Northern Noway and Svalbard with the locations of the extreme values shown in Fig. 6 together with collocated 10-m wind speed from the SAR-only retrieval (**a**) and EC_HRES or AROME-Arctic models (**b**). Land areas and sea ice are masked in **a**. Note that the three images within each frame correspond to different dates and different meteorological conditions.

TABLE I
STATISTICS FOR THE WIND COMPARISONS SHOWN IN FIGURES 6, 8, 9, 11.

speed						
subset	obs vs.	N	mae	bias	corr	rmse
C&R	SAR-only	1919	2.00	0.05	0.79	2.56
	Conventional		1.70	-0.51	0.86	2.25
	EC_HRES		2.15	-1.36	0.77	2.98
	AROME-Arctic		1.81	-0.61	0.83	2.38
IWIN	SAR-only	2265	2.08	1.06	0.65	2.59
	Conventional		1.84	-1.15	0.74	2.35
	EC_HRES		2.65	-2.05	0.57	3.24
	AROME-Arctic		2.24	-0.16	0.58	2.90
direction						
subset	obs vs.	N	mae	bias	corr	rmse
C&R	SAR-only	1919	29.49	1.77	0.61	37.05
	Conventional		21.71	-0.20	0.72	35.89
	EC_HRES		22.32	-1.66	0.73	36.00
	AROME-Arctic		18.63	-0.17	0.78	29.84
	SAR-only$_{clean}$	1605	29.19	1.47	0.58	36.47
IWIN	SAR-only	2265	36.67	-7.12	0.57	47.28
	Conventional		42.56	-3.96	0.48	59.63
	EC_HRES		43.19	-9.54	0.50	59.79
	AROME-Arctic		38.14	-3.09	0.54	57.13
	SAR-only$_{clean}$	2062	33.40	-7.25	0.59	41.94

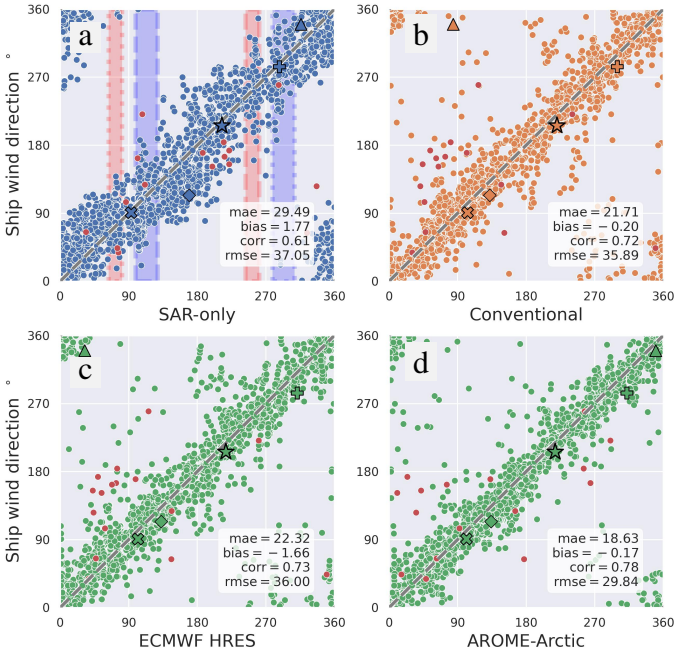

Fig. 8. C&R vessel 10-m wind direction measurements are compared to 10-m wind directions from the SAR-only wind-vector retrieval in blue (**a**, only the closest ambiguity is displayed), to 10-m wind directions from the conventional SAR wind-vector retrieval in orange (**b**), and to NWP model wind directions in green from the global EC_HRES model (**c**), and the regional AROME model (**d**). The red and blue shadings in **a** indicate ascending and descending orbits, respectively, and correspond to all wind directions toward (dotted frame) and away from (dashed frame) the SAR instrument. The grey, dashed, diagonal line indicates perfect match with measured wind. Red dots mark wind directions that correspond to a retrieved wind speed $< 2.4\,\mathrm{m\,s^{-1}}$. The five black-framed symbols and the statistics in the lower right corner of every panel are as in Fig. 6 but with "corr" being the circular correlation coefficient.

wind speed in Isfjorden. On average, the coarse EC_HRES model underestimates *in situ* measurements by -2.05 $\mathrm{m\,s^{-1}}$, whereas AROME-Arctic wind speed shows the smallest wind-speed bias (-0.16 $\mathrm{m\,s^{-1}}$) of all four products, but it frequently overestimates low observed wind speed while underestimating high observed wind speed. AROME-Arctic simulates a similar degree of complexity as is present in the SAR-only retrieved wind field, but both the strongest observed wind speed (star symbol in Fig. 10a,b) and the largest difference between AROME-Arctic and *in situ* measurements (+-symbol Fig. 10 g,h) are associated with small-scale structures that are slightly misrepresented in AROME-Arctic.

It is no surprise that the NWP wind direction (Fig. 11c,d) and thus the wind direction of the conventional wind-vector retrieval (Fig. 11b) perform rather poorly in the vicinity of complex terrain that affects the air flow at smaller scales than are resolved by the NWP models. Therefore, for the IWIN observations inside Isfjorden, wind directions from the SAR-only wind-vector retrieval are clearly superior to wind directions from the NWP models and the conventional wind-vector retrieval (see Tab. I and Fig. 11). This average advantage of the SAR-only wind direction is seen for the complex wind structure in Isfjorden. In waters navigated by C&R vessels, which are less affected by land, this advantage is confined to complex wind fields that are misrepresented by NWP models. The advantage of the SAR-only wind direction persists inside Isfjorden even though known wind direction retrieval errors corresponding to retrieved wind speeds $< 2.4\,\mathrm{m\,s^{-1}}$(red dots) and retrieved directions close to parallel with the look direction of the SAR are not removed (Fig. 11a). Removing retrieved wind speeds $< 2.4\,\mathrm{m\,s^{-1}}$and retrieved wind directions within 3 ° of the radar look direction further improves the wind direction capability of the SAR-only wind-vector retrieval as indicated by SAR-only$_{clean}$ in Table I.

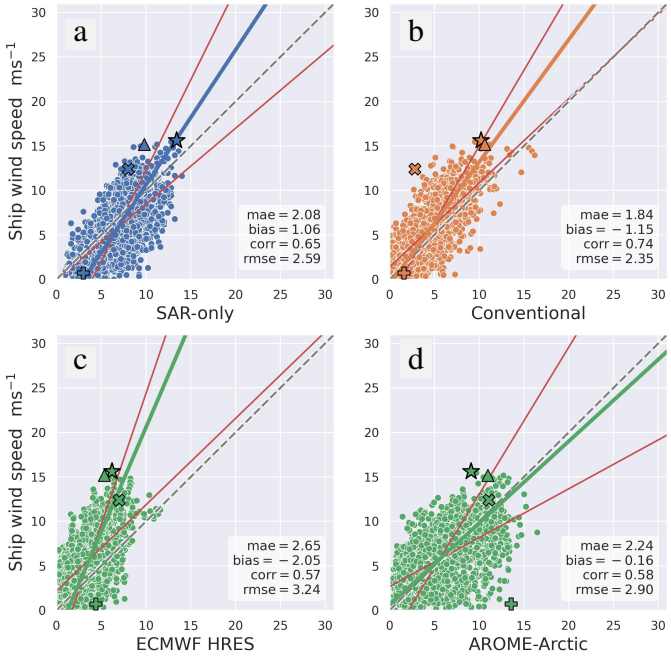

Fig. 9. As Fig. 6 but for 10-m wind speeds measured by the IWIN mobile stations. Black-framed symbols represent the largest *in situ* wind speed observation 15.6 m s^{-1} with stars, the largest difference between conventionally retrieved winds and ship observations (Δ= 9.6 m s^{-1}) with **X**-markers, and the largest differences between ship observations and EC_HRES or AROME with triangles (Δ= 9.8 m s^{-1}) or +-symbols (Δ= 12.9 m s^{-1}), respectively. (a) SAR-only wind-vector retrieval is shown in blue. (b) Conventional SAR wind-vector retrieval in orange. (c) NWP model wind speed is shown in green for the global EC_HRES model. (d) Regional AROME models.

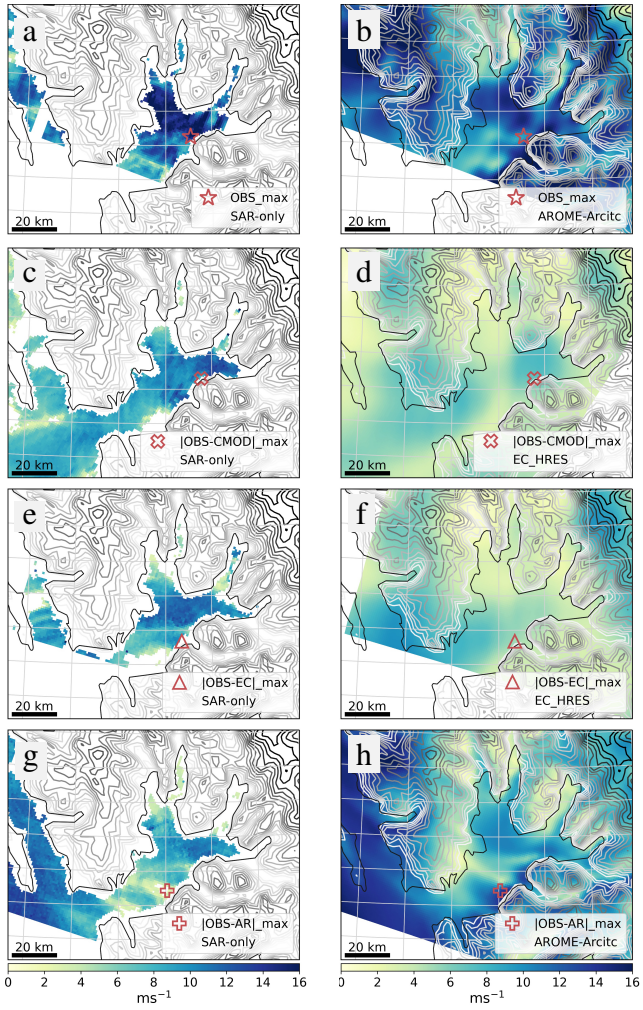

Fig. 10. Map of Isfjorden with the locations of the extreme values shown in Fig. 9 together with collocated SAR-only retrieved 10-m wind speed (**a**), (**c**), (**e**), (**g**), and corresponding NWP simulated wind fields by AROME-Arctic (**b**), (**h**), and EC_HRES (**d**), (**f**).

IV. Discussion

The SAR-only wind-vector retrieval's main advantage over conventional SAR wind-vector retrievals is its independence from other data sources, such as NWP models. This has two major benefits: i) SAR winds can be used as independent observations for validating models and for nowcasting, ii) but, perhaps most importantly, these SAR wind observations can be utilised for data assimilation into NWP models in a similar manner as ambiguous scatterometer winds are already used operationally. Wind fields from SAR-only wind retrieval could enter data assimilation of high-resolution NWP models like AROME-Arctic to improve forecasts of complex weather situations at small scales.

Another positive aspect of the model independence is that the SAR-only retrieval avoids errors that arise from employing an incorrect NWP wind direction, an inherent flaw of conventional SAR wind-vector retrievals that thus far has received little attention. In complex weather conditions with significant small-scale variability of the wind vector field, the conventional SAR retrieval would ***only*** fully exploit the high-resolution capabilities of SAR if accurate auxiliary wind information was provided at the same resolution as the SAR observations which is often not the case. Yet, these are the situations where the high-resolution SAR wind fields are of particular interest for data assimilation into weather forecasting models. Even if one was to model small-scale meteorological features which are resolved by SAR-imagery like e.g., individual convective cells, a slight mismatch between model and SAR of $\mathcal{O}$(1 km) or $\mathcal{O}$(10 min) could lead to virtually any possible wind direction error between model and SAR. This is known as "double penalty error" and describes how errors can double if high resolution structures are misplaced in relation to observations, as opposed to being completely absent from the model wind field. Examples of such errors, that lead to some of the largest discrepancies with *in situ* observations, are visible in Figure 7b and Figure 10b, h. Conventional wind-vector retrievals perform best with moderate-resolution auxiliary wind direction input because the risk of double penalty errors, in which high-resolution structures are slightly misplaced in space or time, increases with model resolution. As a direct consequence of avoiding double penalty errors, the SAR-only retrieval performs well for complex wind fields at open sea (Figs. 6-7) and for terrain-induced flow in coastal areas (Figs. 9-10). The same was found for dynamically changing weather situations that are associated with large wind gradients, such as polar lows [11].

The combination of co-pol and cross-pol backscatter in the SAR-only method improves the retrieval of strong winds com-

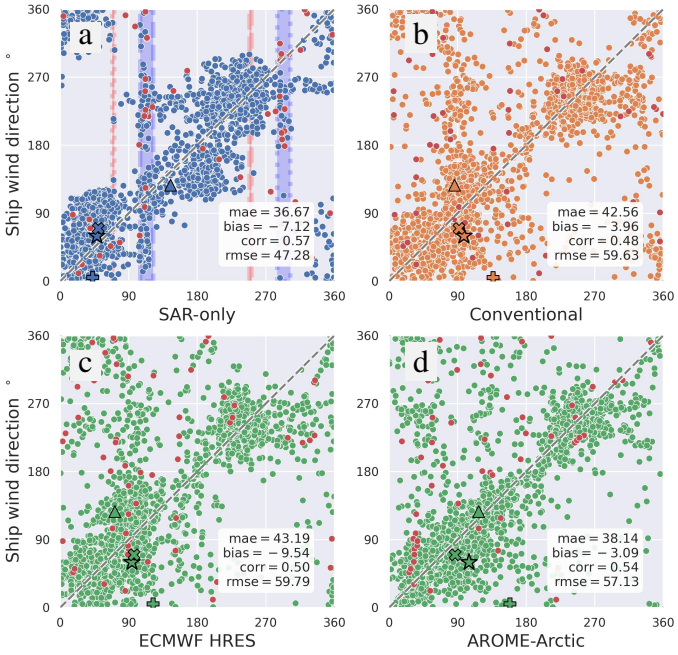

Fig. 11. As Fig. 8 but for 10-m wind directions measured by IWIN mobile stations. (a) SAR-only wind-vector retrieval is shown in blue. (b) Conventional SAR wind-vector retrieval in orange. (c) NWP model wind direction is shown in green for the global EC_HRES model. (d) Regional AROME models.

pared to the conventional method which is known to become progressively incorrect at wind speeds exceeding $20\,\mathrm{m\,s^{-1}}$due to saturation of the co-pol backscatter signal at high wind speeds. Close to signal saturation, the conventional method becomes extremely sensitive to the auxiliary wind direction from NWP or changes in the backscatter intensity. Even small errors in the auxiliary wind direction can therefore result in large errors of the wind vector retrieved with the conventional method. Figure 6 illustrates this pattern despite the fact that there are few high wind observations. IWIN *in situ* observations from the three tourist fjord-cruise ships on Svalbard, which steer clear of severe winds, do not demonstrate this advantage of combining co-pol and cross-pol backscatter.

Aside from the discussed advantages of the SAR-only retrieval, a number of challenges remain at this stage. Among these are the current limitation of SAR-only retrieval to retrieve wind vectors in weak-wind conditions; and related to this, the retrieved wind direction's tendency to incorrectly align with directions towards and away from the SAR at low wind speed; contamination due to the inaccuracy of the valid-data mask contained in the OCN product; an inadequate treatment of error terms in the costfunction; and the lack of a sophisticated ambiguity removal technique to produce an unambiguous wind field.

DCA is calculated from the DC data contained in ESA's Sentinel-1 Level-2 OCN product by subtracting the median DC over land (a static reference) from DC data over water. The approach of calculating DCA using interpolated DC values does not seem to further degrade DCA data quality, which is already the lowest of the three data sources that enter SAR-only retrieval. Improving the quality of DCA data for SAR-only wind-vector retrieval is expected to improve the SAR-only retrieval as a whole, especially at low wind speed. As mentioned in section II-A2, DCA provides information on the wind vector component parallel with the range direction v_{rDP}, hence towards or away from the SAR, while σ^0_{CoP} and σ^0_{XP} contain mainly information about the wind speed $|\mathbf{v}|$. Since $\pm\frac{v_{\mathrm{rDP}}}{|\mathbf{v}|} = \cos\theta$, as illustrated in Figure 5 (where the sign is dependent on the flight direction of the SAR), the SAR-only retrieval of the wind direction θ is more sensitive to measurement errors if the wind direction is close to aligned with the range direction and $\frac{v_{\mathrm{rDP}}}{|\mathbf{v}|} \approx 1$. In addition, the quality of the SAR-only wind retrieval is generally limited in weak wind conditions since the uncertainty of the wind component in range direction Δv_{rDP}, caused by the DCA error, becomes of similar magnitude as $|\mathbf{v}|$, and the retrieved wind direction becomes primarily a result of the DCA error and hence aligned with the look direction. When all SAR-only wind speeds below $2.4\,\mathrm{m\,s^{-1}}$and retrieved wind directions within $\pm 3\,^\circ$ of the range direction are excluded from the IWIN data set, incorrectly aligned wind directions towards and away from the SAR in Figure 11 almost entirely vanish (not shown) and wind direction statistics of the SAR-only retrieval further improved (see $\mathrm{SAR\text{-}only}_{\mathrm{clean}}$ in Tab. I). For the data set from the C&R vessels, which contains only three wind speed observations below $1\,\mathrm{m\,s^{-1}}$, improving DCA calibration by using the interpolation technique introduced in Section II-A2 instead of a polynomial fit lead to a strong reduction of false wind direction alignment with the range direction (Figure 8a).

Here, we relied mostly on ESA's Sentinel-1 Level-2 OCN product since it contains all three input fields to the SAR-only retrieval, σ^0_{CoP} and σ^0_{XP} as well as DC. However, the somewhat inaccurate valid data mask close to the coast and the sea-ice edge as well as the DC data set might be replaced with higher quality data to reduce errors of the SAR-only retrieval.

Methods that use wind-aligned linear features in SAR images to infer wind direction [40, 41] may improve SAR-only retrieval by providing additional information to the DCA which is now the primary source of wind direction information, and by removing directional ambiguity. Additionally, a careful investigation aimed at substituting the constant error terms $\Delta\sigma_{\mathrm{CoP}}$, $\Delta\sigma_{\mathrm{XP}}$, and ΔDCA in the costfunction (Eqn. 4) with variable errors may lead towards an optimal use of the information contained in SAR images and restore the original role of error terms in the probabilistic wind-vector retrieval.

V. Conclusion

A SAR-only wind-vector retrieval that combines co-pol and cross-pol SAR backscatter with Doppler centroid anomaly (DCA) to obtain the full wind vector has recently been proposed [11]. Here, over 4,000 *in situ* wind measurements collected by 10 different ships from March 2021 to October 2022 are used to validate 10-m wind vectors from a current version of this SAR-only retrieval. These retrieved vectors are then compared to 10-m wind from two NWP models and the conventional SAR wind-vector retrieval method, which relies on prior auxiliary wind information from one of the NWP models. Furthermore, a new substitution method to calibrate

the DCA for wind retrieval is tested for SAR scenes without land pixels. These are the main findings:

- High-resolution surface wind fields obtained from the unsupervised SAR-only wind-vector retrieval are of similar quality compared to the conventional model-dependent wind-vector retrieval at open sea where the 10-m wind field is unperturbed by coastal topography.
- In the vicinity of complex coastal topography, for high wind speed, and in complex meteorological situations, the SAR-only wind-vector retrieval appears to outperform the standard wind-vector retrieval and NWP models, especially as concerns wind direction.
- The quality of SAR-only wind-vector retrieval does not appear to be degraded by interpolating median DC values for the DCA calibration.

Ambiguous wind vectors from the unsupervised SAR-only retrieval have proven to be of at least similar quality as the model-dependent standard wind-vector retrieval method and NWP simulations. Therefore, future studies should asses the impact assimilating independent SAR-only wind observations into a high-resolution NWP model.

Acknowledgments

Many thanks to Lukas Frank and Marius Jonassen at the University Center in Svalbard, who set up the observational network in Isfjorden (IWIN) and provided assistance with this work's development by processing the wind measurements and responding to inquiries. We would also want to express our gratitude to the Norwegian Coast Guard for granting us access to the wind observations obtained by three of their vessels and for sailing through all the strongest wind speeds reported in this study. We also want to acknowledge contributions by Eirik Mikal Samuelsen from the Norwegian Meteorological institute to facilitating access to the Coast Guard observations and forming the initial idea for this manuscript, and by Harald Johnsen who adviced the formulation of the SAR-only retrieval concept.

Appendix
Formulation of the smooth weighing function

The first two terms in Equation 1 contain a weighing function $w(\theta, \sigma^0_{\mathrm{XP}})$. The purpose of this weighing function is to give all weight to the co-pol term of Equation 1 with $w(\theta, \sigma^0_{\mathrm{XP}}) = 0$ for wind speed below $4\,\mathrm{m\,s^{-1}}$, and to the cross-pol term in Equation 1 with $w(\theta, \sigma^0_{\mathrm{XP}}) = 1$ for wind speed larger than $20\,\mathrm{m\,s^{-1}}$. For wind speeds between $4\,\mathrm{m\,s^{-1}}$and $20\,\mathrm{m\,s^{-1}}$weight should be distributed according to the polynomial step function $3x^2 - 2x^3$. To achieve this the GMF MS1A [5] is used to calculate $\sigma^0_{\mathrm{XPmin}}$ and $\sigma^0_{\mathrm{XPmax}}$ values that correspond to $u_{min} = 4\,\mathrm{m\,s^{-1}}$and $u_{max} = 20\,\mathrm{m\,s^{-1}}$for the given incidence angle θ. Then the weight is calculated evaluating the polynomial

$$w(\theta) = 3x^2 - 2x^3$$

where

$$x = \left\{ \begin{array}{ll} 0, & \text{for } \sigma^0_{\mathrm{XP}} < \sigma^0_{\mathrm{XPmin}} \\ 1, & \text{for } \sigma^0_{\mathrm{XP}} > \sigma^0_{\mathrm{XPmax}} \\ \dfrac{\sigma^0_{\mathrm{XP}} - \sigma^0_{\mathrm{XPmin}}}{\sigma^0_{\mathrm{XPmax}} - \sigma^0_{\mathrm{XPmin}}}, & \text{else} \end{array} \right\}.$$

Figure 12 shows the resulting weighing function $w(\theta, \sigma^0_{\mathrm{XP}})$ for relevant θ and σ^0_{XP} ranges.

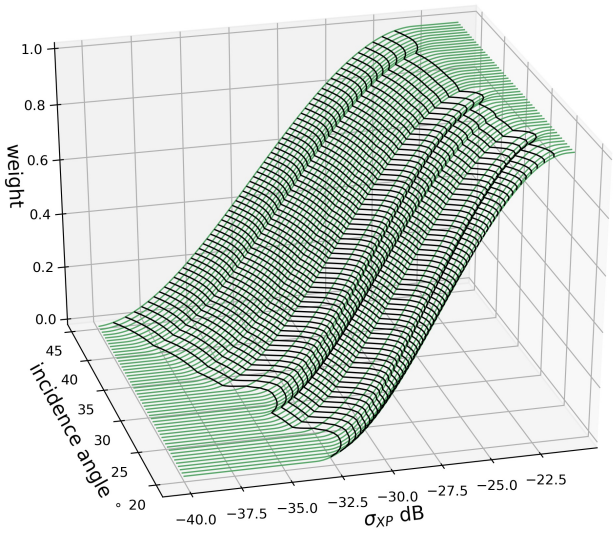

Fig. 12. Smooth step function for the weights of the cross-pol, and co-pol terms.

References

[1] ESA, "Sentiel-1 Technical Guide," https://sentinel.esa.int/web/sentinel/ocean-wind-field-component, 2023, accessed 19 January 2023.

[2] M. Portabella, A. Stoffelen, and J. A. Johannessen, "Toward an optimal inversion method for synthetic aperture radar wind retrieval," *Journal of Geophysical Research: Oceans*, vol. 107, no. C8, pp. 1–1, 2002.

[3] H. Hersbach, "Comparison of C-band scatterometer CMOD5. N equivalent neutral winds with ECMWF," *Journal of Atmospheric and Oceanic Technology*, vol. 27, no. 4, pp. 721–736, 2010.

[4] P. W. Vachon and J. Wolfe, "C-band Cross-Polarization Wind Speed Retrieval," *IEEE Geoscience and Remote Sensing Letters*, vol. 8, no. 3, pp. 456–459, 2010.

[5] P. A. Hwang, A. Stoffelen, G.-J. van Zadelhoff, W. Perrie, B. Zhang, H. Li, and H. Shen, "Cross-polarization geophysical model function for C-band radar backscattering from the ocean surface and wind speed retrieval," *Journal of Geophysical Research: Oceans*, vol. 120, no. 2, pp. 893–909, 2015.

[6] A. A. Mouche, B. Chapron, B. Zhang, and R. Husson, "Combined Co- and Cross-Polarized SAR Measurements Under Extreme Wind Conditions," *IEEE Transactions on Geoscience and Remote Sensing*, vol. 55, no. 12, pp. 6746–6755, 2017.

[7] B. Zhang, A. Mouche, Y. Lu, W. Perrie, G. Zhang, and H. Wang, "A Geophysical Model Function for Wind Speed Retrieval From C-Band HH-Polarized Synthetic Aperture Radar," *IEEE Geoscience and Remote Sensing Letters*, vol. 16, no. 10, pp. 1521–1525, 2019.

[8] P. J. Stoll, T. M. Valkonen, R. G. Graversen, and G. Noer, "A well-observed polar low analysed with a regional and a global weather-prediction model," *Quarterly Journal of the Royal Meteorological Society*, vol. 146, no. 729, pp. 1740–1767, 2020.

[9] E. A. Rasmussen, "Polar Lows," in *A Half Century of Progress in Meteorology: A Tribute to Richard Reed*. Springer, 2003, pp. 61–78.

[10] M. Mile, R. Randriamampianina, G.-J. Marseille, and A. Stoffelen, "Supermodding – A special footprint operator for mesoscale data assimilation using scatterometer winds," *Quarterly Journal of the Royal Meteorological Society*, vol. 147, no. 735, pp. 1382–1402, 2021.

[11] M. Tollinger, R. Graversen, and H. Johnsen, "High-Resolution Polar Low Winds Obtained from Unsupervised SAR Wind retrieval," *Remote Sensing*, vol. 13, no. 22, p. 4655, 2021.

[12] B. Zhang and W. Perrie, "Cross-Polarized Synthetic Aperture Radar: A New Potential Measurement Technique for Hurricanes," *Bulletin of the American Meteorological Society*, vol. 93, no. 4, pp. 531–541, 2012.

[13] G. Zhang, X. Li, W. Perrie, P. A. Hwang, B. Zhang, and X. Yang, "A Hurricane Wind Speed Retrieval Model for C-Band RADARSAT-2 Cross-Polarization ScanSAR Images," *IEEE Transactions on Geoscience and Remote Sensing*, vol. 55, no. 8, pp. 4766–4774, 2017.

[14] R. D. Lindsley, J. R. Blodgett, and D. G. Long, "Analysis and Validation of High-Resolution Wind from ASCAT," *IEEE Transactions on Geoscience and Remote Sensing*, vol. 54, no. 10, pp. 5699–5711, 2016.

[15] B. Lin, W. Shao, X. Li, H. Li, X. Du, Q. Ji, and L. Cai, "Development and validation of an ocean wave retrieval algorithm for VV-polarization Sentinel-1 SAR data," *Acta Oceanologica Sinica*, vol. 36, pp. 95–101, 2017.

[16] H. Wang, J. Yang, A. Mouche, W. Shao, J. Zhu, L. Ren, and C. Xie, "GF-3 SAR Ocean Wind Retrieval: The First View and Preliminary Assessment," *Remote Sensing*, vol. 9, no. 7, p. 694, 2017.

[17] J.-C. Jang, K.-A. Park, A. A. Mouche, B. Chapron, and J.-H. Lee, "Validation of Sea Surface Wind From Sentinel-1A/B SAR Data in the Coastal Regions of the Korean Peninsula," *IEEE Journal of Selected Topics in Applied Earth Observations and Remote Sensing*, vol. 12, no. 7, pp. 2513–2529, 2019.

[18] Y. Lu, B. Zhang, W. Perrie, A. Mouche, and G. Zhang, "CMODH Validation for C-Band Synthetic Aperture radar HH Polarization Wind Retrieval Over the Ocean," *IEEE Geoscience and Remote Sensing Letters*, vol. 18, no. 1, pp. 102–106, 2020.

[19] B. Zhang, Y. Lu, W. Perrie, G. Zhang, and A. Mouche, "Compact Polarimetry Synthetic Aperture Radar Ocean Wind Retrieval: Model Development and Validation," *Journal of Atmospheric and Oceanic Technology*, vol. 38, no. 4, pp. 747–757, 2021.

[20] M. Müller, Y. Batrak, J. Kristiansen, M. A. Køltzow, G. Noer, and A. Korosov, "Characteristics of a Convective-Scale Weather Forecasting System for the European Arctic," *Monthly Weather Review*, vol. 145, no. 12, pp. 4771–4787, 2017.

[21] M. B. Christiansen, W. Koch, J. Horstmann, C. B. Hasager, and M. Nielsen, "Wind resource assessment from C-band SAR," *Remote Sensing of Environment*, vol. 105, no. 1, pp. 68–81, 2006.

[22] A. Bentamy, A. Mouche, A. Grouazel, A. Moujane, and A. A. Mohamed, "Using sentinel-1A SAR wind retrievals for enhancing scatterometer and radiometer regional wind analyses," *International Journal of Remote Sensing*, vol. 40, no. 3, pp. 1120–1147, 2019.

[23] H. Wang, H. Li, M. Lin, J. Zhu, J. Wang, W. Li, and L. Cui, "Calibration of the Copolarized Backscattering Measurements From Gaofen-3 Synthetic Aperture Radar Wave Mode Imagery," *IEEE Journal of Selected Topics in Applied Earth Observations and Remote Sensing*, vol. 12, no. 6, pp. 1748–1762, 2019.

[24] B. Zhang and W. Perrie, "Recent progress on high wind-speed retrieval from multi-polarization SAR imagery: a review," *International Journal of Remote Sensing*, vol. 35, no. 11-12, pp. 4031–4045, 2014.

[25] T. Ahsbahs, M. Badger, I. Karagali, and X. G. Larsén, "Validation of Sentinel-1A SAR Coastal Wind Speeds Against Scanning LiDAR," *Remote Sensing*, vol. 9, no. 6, p. 552, 2017.

[26] R. Brown, "On satellite scatterometer model functions," *Journal of Geophysical Research: Atmospheres*, vol. 105, no. D23, pp. 29 195–29 205, 2000.

[27] B. R. Furevik, O. M. Johannessen, and A. D. Sandvik, "SAR-retrieved wind in polar regions-comparison with in situ data and atmospheric model output," *IEEE Transactions on Geoscience and Remote Sensing*, vol. 40, no. 8, pp. 1720–1732, 2002.

[28] Norwegian Meteorological Institute, "Frost API," https://frost.met.no/index.html, 2022, accessed 01 November 2022.

[29] L. Frank, M. O. Jonassen, T. Remes, F. R. Schalamon, and A. Stenlund, "Iwin: The isfjorden weather information network," pp. 1–19, 2023.

[30] A.-M. Olsen, M. Øiestad, E. Berge, M. Ø. Køltzow, and T. Valkonen, "Evaluation of Marine Wind Profiles in the North Sea and Norwegian Sea Based on Measurements and Satellite-Derived Wind Products," *Tellus*, vol. 74, no. 1, p. 1, 2022.

[31] H. Charnock, "A note on empirical wind-wave formulae," *Quarterly Journal of the Royal Meteorological Society*, vol. 84, no. 362, pp. 443–447, 1958.

[32] ESA, "Sentiel-1 Technical Guide," https://sentinel.esa.int/web/sentinel/missions/sentinel-1, 2023, accessed 19 January 2023.

[33] ——, "Copernicus Sentinel-1 A/B Level-2 OCN," 2021-2022, retrieved from ASF DAAC November, 2022, https://search.asf.alaska.edu/#/ processed by ESA.

[34] T. Haiden, M. Janousek, J. Bidlot, L. Ferranti, F. Prates, F. Vitart, P. Bauer, and D. Richardson, *Evaluation of ECMWF forecasts, including the 2016 resolution upgrade*. European Centre for Medium Range Weather Forecasts Reading, UK, 2016.

[35] ESA, "Sentinel-1 IPF Auxiliary Product Specification," https://sentinels.copernicus.eu/documents/247904/1877131/DI-MPC-PB-0241-3-10_Sentinel-1IPFAuxiliaryProductSpecification.pdf/ae025687-c3e3-6ab0-de8d-d9cf58657431?t=1669115416469, 2022, accessed 20 January 2023.

[36] M. Müller, M. Homleid, K.-I. Ivarsson, M. A. Køltzow, M. Lindskog, K. H. Midtbø, U. Andrae, T. Aspelien, L. Berggren, D. Bjørge *et al.*, "AROME-MetCoOp: A Nordic Convective-Scale Operational Weather Prediction Model," *Weather and Forecasting*, vol. 32, no. 2, pp. 609–627, 2017.

[37] ESA, "Sentinel-1 Annual Performance Report 2022," https://sentinel.esa.int/documents/247904/4889382/DI-MPC-APR-0588-1-2-track-Annual+Performance+Report+2022.pdf/a683c9d2-06c2-9143-b456-4a9c8e30e449?t=1678771841042, 2022, accessed 07 November 2023.

[38] F. Said, H. Johnsen, B. Chapron, and G. Engen, "An Ocean Wind Doppler Model Based on the Generalized Curvature Ocean Surface Scattering Model," *IEEE transactions on geoscience and remote sensing*, vol. 53, no. 12, pp. 6632–6638, 2015.

[39] A. A. Mouche, F. Collard, B. Chapron, K.-F. Dagestad, G. Guitton, J. A. Johannessen, V. Kerbaol, and M. W. Hansen, "On the Use of Doppler Shift for Sea Surface Wind Retrieval From SAR," *IEEE Transactions on Geoscience and Remote Sensing*, vol. 50, no. 7, pp. 2901–2909, 2012.

[40] Y. Du, P. W. Vachon, and J. Wolfe, "Wind direction estimation from SAR images of the ocean using wavelet analysis," *Canadian Journal of Remote Sensing*, vol. 28, no. 3, pp. 498–509, 2002.

[41] W. Koch, "Directional analysis of SAR images aiming at wind direction," *IEEE Transactions on Geoscience and Remote Sensing*, vol. 42, no. 4, pp. 702–710, 2004.